M. D. Barringer
e-mail: mbarringer@psu.edu

K. A. Thole
e-mail: kthole@psu.edu

D. L. Breneman
e-mail: dbreneman@usboiler.net

Mechanical and Nuclear Engineering Department,
Pennsylvania State University,
University Park, PA 16802

K.-M. Tham
e-mail: kokmun.tham@siemens.com

V. Laurello
e-mail: vincent.laurello@siemens.com

Siemens Energy,
Orlando, FL 32826

Effects of Centrifugal Forces on Particle Deposition for a Representative Seal Pin Between Two Blades

Many land-based gas turbine applications are conducive to the formation of rust in the supply piping and other components that are upstream of the gas turbine. Many of these applications do not incorporate an effective filtration system for removing rust particles from the secondary air systems thereby resulting in rust deposits. Deposits in the small passages significantly block the secondary flow that ultimately reduces component life. This study investigates the effects of rust deposition in a geometry representative of an axial seal pin between two blades. Initial studies were performed to determine the effects of engine-representative particle composition, temperature, and centrifugal acceleration on deposition characteristics. These initial results pointed to the importance of simulating centrifugal forces representative of that experienced in the engine. A new facility was developed to directly measure flow blockages under static conditions and under rotational conditions. [DOI: 10.1115/1.4007751]

Introduction

Current land-based engines have turbine inlet gas temperatures around 1400 °C while prototype turbines are being developed for operation with inlet temperatures up to 1600 °C [1,2]. High-pressure air is bled from the compressor and used to cool components and to minimize hot gas ingestion. As shown in Fig. 1, air supplied from beneath the blade platform is used for blade cooling and to prevent ingestion of the hot gas flow into gaps such as those between adjacent blades. Deposition of particles in the secondary flow passages causes reduction of flow and inhibits the function of structural components. These small particles result from intake conditions as well as rust buildup in supply pipes.

Land-based gas turbines typically use large external filters to remove particles from the air flow, though cyclone separation offers an alternative to filters. Studies have shown that cyclones become less effective for particles smaller than 10 μm [3–5]. Due to the challenge of filtering small particles and the decline of filter performance over time, some particulate matter remains entrained in the air as it enters the turbine. Several studies have measured particulate concentrations in the cooling air of an operating turbine [6–10]. Their results indicated that particles entering the turbine internal air system can be of sufficient size to block air flow passages.

Particulate matter is of special concern during turbine startup, when high concentrations of particles such as rust are present in the cooling air flow [11]. This problem is exacerbated by the tendency to use gas turbines intermittently due to their operational flexibility in power generation. During offline times, components such as carbon steel piping external to the engine can rust significantly. This rust is subsequently entrained in the cooling air flow and deposited throughout the air flow path.

One particular location where rust particles can deposit is at the axial seal pin between two adjacent blade platforms. The axial seal pin is loosely held in place by an oversized slot in the side of the blade platform. During operation of the turbine, centrifugal acceleration forces the pin radially outward against the slot, which creates a partial seal that prevents excessive leakage of high-pressure secondary air into the hot gas flow. The seal pin also functions as a mobile vibration damper. Rust particles can deposit around the seal pin, preventing its movement and inhibiting its function as a vibration damper.

To the author's knowledge, no previous studies have investigated rust particle ingestion and deposition. Since rust, which is mostly iron oxide, differs considerably from sand, comprised mainly of silicon dioxide, effects of rust particle ingestion may differ from those previously reported for sand. For example, the density of rust is about 5200 kg/m^3, which is nearly twice that of sand, about 2650 kg/m^3. This density difference may cause rust particles of a given size to exhibit more inertial behavior than similarly sized sand particles. In addition, rust particles are softer than sand and are, therefore, more easily crushed, which could influence particle behavior on impact with a solid surface.

The objective of the present study is to understand the effects of particle deposition in a test geometry representative of the axial seal pin between two adjacent blade platforms. Simple particle characterization tests were performed to identify the dominant factors influencing particle behavior such as temperature, compaction, pressure ratio, and rotation. This paper first reports the results of simple static tests that identified the primary influence on particle deposition that occurs in actual engine operations.

Scaling of Engine to Lab Conditions

Since complete turbine engine conditions cannot be simulated in a laboratory environment, the scaling of relevant parameters was considered. The dependent effects that were desired included the temperature of the particles, the pressure ratio, and rotation. The independent parameters were considered to be the seal pin geometry, particle sizes, and the variation in the rotational speeds.

For the static tests, the turbine blades used were the actual engine hardware found in an industrial gas turbine engine and, therefore, the seal pin geometry was identical to the engine. For the rotational tests, it was not possible to spin the entire engine turbine blades due to weight constraints. As such, a segment of the platform geometry was used from the engine blade static tests.

Contributed by the International Gas Turbine Institute (IGTI) of ASME for publication in the JOURNAL OF ENGINEERING FOR GAS TURBINES AND POWER. Manuscript received June 19, 2012; final manuscript received September 1, 2012; published online February 11, 2013. Editor: Dilip R. Ballal.

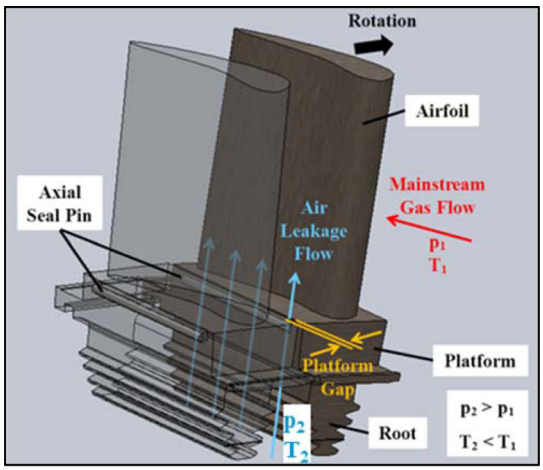

(A)

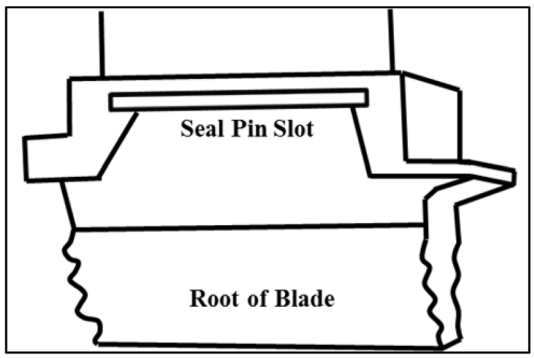

(B)

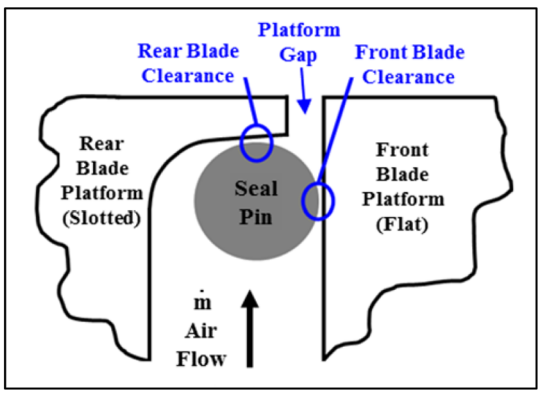

(C)

Fig. 1 (*a*) Illustration of the leakage flow through the blade platform between two blades, (*b*) schematic illustrating the seal pin region, and (*c*) schematic showing the cross section of the seal-pin and blade platforms

The rotational tests used the same geometry with only one-fourth of the seal pin length of the blade ($L_{sp,rotational} = 1/4\ L_{sp,static} = 1/4\ L_{sp,engine}$).

Test particles similar to rust deposits at the axial seal pin in a field-run turbine were created from a mixture of commercial metal powders. The test particles were relatively loose and of a powder-like, granular consistency. Particles were composed of 86% red iron oxide (Fe_2O_3) and 10% zinc oxide (ZnO) along with several trace metal oxide compounds. As shown in Fig. 2, the size distribution of the particles created in the laboratory was similar to that

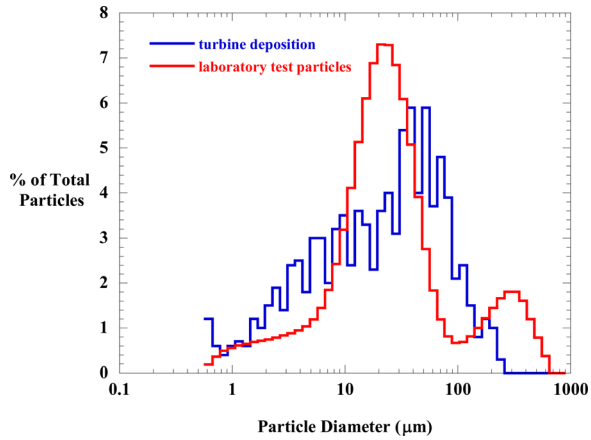

Fig. 2 Size distributions for rust particles from turbine deposition samples and the laboratory test particles

for the turbine samples. The particle sizes were measured using a dry laser diffraction technique. The median particle diameters from field run turbine components as well as the laboratory particles were 19 μm and 20 μm, respectively.

The centrifugal acceleration to be matched to that of an industrial turbine required 12,100 times sea-level gravitational acceleration. For the industrial gas turbine matched in this study, the first row platform radius, which is just above the axial seal pin slot, is nominally 850 mm. Using this radius and the base load engine speed of 3600 rpm, the relative centrifugal force (RCF) was calculated to be 12,100 times gravitational acceleration using Eq. (1), where r is the radius, ω is rotating speed, and g is gravitational acceleration.

$$\mathrm{RCF} = \frac{r\omega^2}{g} \tag{1}$$

For initial tests evaluating whether rotational effects were of importance, particle samples were spun in a Beckman Coulter Avanti J-25 centrifuge using the JA-25.50 rotor. The outer radius of the sample tube from the axis of rotation was 108 mm; therefore, rotational speeds of 10,000 rpm were required to generate the centrifugal accelerations. For the full testing on rotational effects (facility described later in this paper), the components required a rotational speed of 10,300 rpm, which was achieved by the centrifuge.

Effects of Temperature on Rust Particles. Rust particles, containing 86% red iron oxide (Fe_2O_3) and 10% zinc oxide (ZnO) as well as other particle compositions including sand (SiO_2) and black iron oxide (Fe_2O_3), were heated in a kiln at 222 °C/hr to turbine representative gas and metal temperatures ranging from 540 °C to 1093 °C. The test particles are summarized in Table 1. During these experiments, particles were observed for changes in color and conglomeration. Analysis of the particles after heating was performed using laser diffraction to check for changes in size distribution. The particle composition was measured using an environmental scanning electron microscope (ESEM) with energy dispersive X-ray spectroscopy. Since the particle composition remained unchanged after heating, it was concluded that particles

Table 1 Composition of various particles

Product	Mass %	Melting temp (°C)
Red iron (III) oxide, Fe_2O_3	86.3	1538
Zinc oxide, ZnO	10.2	1975

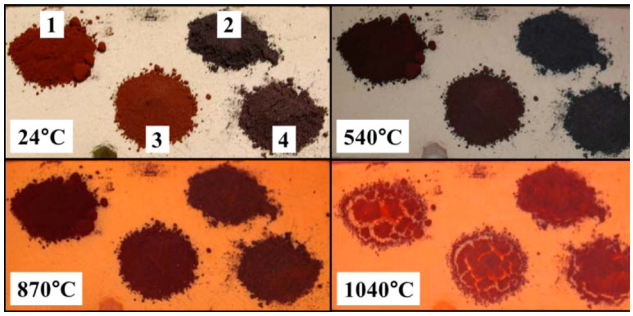

Fig. 3 Rust particles at room temperature and during heating. Sample compositions: (1) 100% red Fe_2O_3; (2) 100% black Fe_2O_3; (3) 90% red Fe_2O_3, 10% Al_2O_3; (4) 45% red Fe_2O_3, 45% black Fe_2O_3, 10% Al_2O_3.

were not contaminated while exposed to the laboratory environment during heating.

As shown in Fig. 3, particles formed large agglomerations at temperatures above 950 °C. This effect was most significant for particles composed primarily of red Fe_2O_3. Since heating temperatures did not exceed particle melting temperatures, it was possible to break up agglomerations after the particles cooled to the ambient.

Red Fe_2O_3 samples turned completely black at temperatures in excess of 1000 °C, which was indicative of a phase change. Effects of color change and conglomeration remained after heated samples cooled back to the ambient temperature. Particles at the center of each sample required more time to heat due to the insulating effect of the surrounding particles so, therefore, increased exposure time was required for complete heating of the sample. This effect was observed through a slight increase in the particle size distribution as exposure time was increased from 0 to 120 min. When the test particles were heated to temperatures typical of the first row blade root, about 850 °C, there was no color change, conglomeration, or increase in particle size. In all cases, after heating to 850 °C, it was possible to break up the samples of rust that were heated.

Effects of Centrifugal Forces on Rust Compaction. In separate experiments, rust particles were spun in a centrifuge at room temperature (21 °C) and at centrifugal accelerations matched to those in an engine, approximately 12,100 times gravitational acceleration. Particles were placed inside sample containers and then positioned within the centrifuge. The bulk density of the particles was measured by a volume displacement method before and after centrifuging to quantify the compaction of particles.

Centrifuging doubled the bulk density of the particles relative to their unprocessed loose state. The forces caused particles to agglomerate into a single compacted mass that adhered to the radially outermost side of the containment tube. The centrifuged particles were removed from the sample holder by vigorously striking the tube to break up the compacted mass. As shown in Fig. 4, large conglomerations of particles remained after removal.

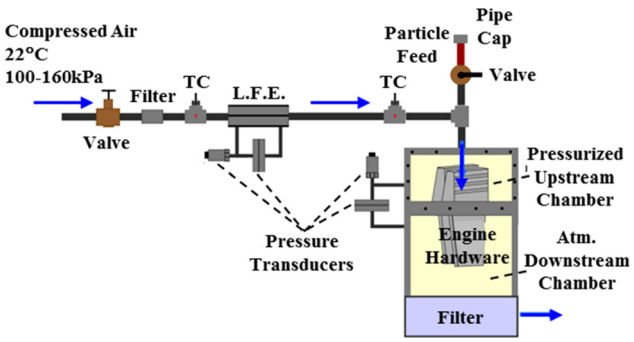

Fig. 5 Schematic of the static test facility

Based on the heating results and the results from the centrifuge tests, it was determined that the engine-representative centrifugal acceleration effects dominated those of the heating effects. This finding provided impetus to include rotation in experiments designed to investigate particle deposition and flow blockage at the axial seal pin.

Description of Two Test Facilities

Following the initial tests that identified a dominant factor of centrifugal forces, two test facilities were developed to investigate the effects of rust particles under static and rotational conditions on seal pin flow blockage. Shown schematically in Fig. 5, the static test facility flowed compressed air through the engine hardware at laboratory ambient temperatures. This test facility provided the means to inject rust particles into the airstream upstream of the turbine blade platform. The primary components of the static test facility included a compressed air supply, laminar flow element (LFE), upstream and downstream test chambers containing the engine hardware, and a gravity-feed particle injection system.

Air from a remote compressor was supplied to the stationary test facility at approximately 410 kPa gauge and 22 °C. At the inlet to the test facility, a pressure regulating valve was used to set the upstream air pressure between 100 and 160 kPa. A laminar flow element was used to measure the needed flow rate for the experiment that varied from 60 cm^3/s to 400 cm^3/s at standard conditions.

Flow of gas through a nozzle or diffuser can be approximated as one-dimensional, isentropic flow of an ideal gas, which permits definition of a nondimensional flow parameter that can be used to predict the flow through a nozzle or diffuser if the upstream total to downstream static pressure ratio P_0/p_b is known. For the tests under consideration in this study, the experimental setup consisted

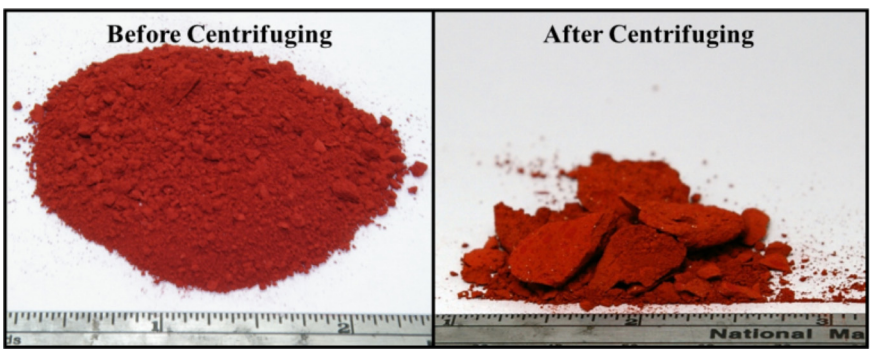

Fig. 4 Rust particles before and after centrifuging

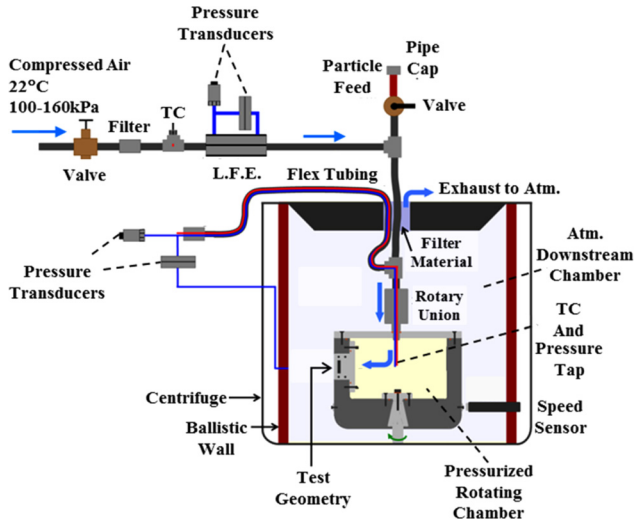

Fig. 6 Schematic of the rotating test facility

of a relatively large upstream plenum followed by a narrow flow area at the seal pin in which the flow exhausted to the atmosphere.

The pressurized upstream chamber acted as a plenum due to its large cross-sectional area relative to the seal pin flow area. Thus, an absolute pressure transducer connected to the upstream chamber was used to measure the upstream total air pressure. Just upstream of the chamber a thermocouple was used to measure the air temperature. This temperature in conjunction with the air mass flow rate and upstream total pressure was used to calculate the flow function FF. A differential pressure transducer measured the pressure drop across the seal pin, which allowed the pressure ratio across the engine hardware to be calculated. The pressure ratio PR was calculated as the ratio of the upstream chamber pressure P_0 to the downstream chamber pressure at atmospheric conditions p_b. Rust was introduced through a sealed pipe in which gravity was used to instantaneously inject the rust into the compressed air, as shown in Fig. 5.

The rotating test facility, shown schematically in Fig. 6, was designed to flow compressed air and rust particles through representative test coupons of the blade platform gap and seal pin. To reduce the size and mass of the rotating components, test coupons representative of the seal pin geometry were manufactured to represent one-fourth of the engine, true-scale length of the blade platform. The coupon included the seal pin slot, seal pin, and the contoured surface between the seal pin slot and the root. Components of the rotating test facility were similar to the stationary facility with the addition of a variable-speed centrifuge modified to spin the test geometries and a rotary coupling for the air supply. The rotating facility was capable of matching the centrifugal acceleration in a gas turbine, about 12,100 times gravitational acceleration.

As indicated in Fig. 6, only the pressurized chamber and test geometries rotated while all other components remained stationary. Similar to the setup in the stationary test facility, the particle injection system was connected to the top of the tee fitting and consisted of a vertical 20 cm long pipe with a sealed cap at the top and ball valve at the bottom. From this tee fitting, air and particles passed through a 30 cm long flexible tube to the top of a second tee fitting, which was connected through the rotary coupling to the top of the rotating chamber. The rotary coupling allowed air from the LFE and particles to enter the rotating chamber with no leakage. To provide containment in the event of accidental liberation of rotating components, the rotating chamber and rotary union were entirely contained inside the metal-encased centrifuge shield made of 12.7 mm thick steel. A sensor was mounted onto the ballistic shield to monitor the rotating speed.

As shown in Fig. 7, a rotating chamber was designed to have three ports through the side wall for three coupons. To improve

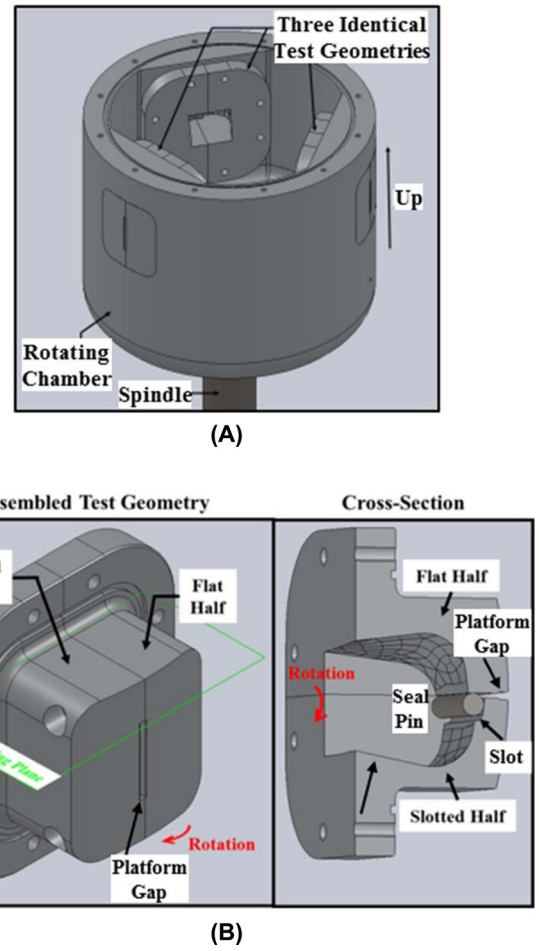

Fig. 7 Illustration of (*a*) rotating test chamber designed to spin three identical test pieces representative of the engine seal pin and platform gap region shown in (*b*)

balance and increase the amount of data, three identical coupons were installed in these ports. Each test coupon consisted of two separable halves representative of two adjacent blade platforms. Each of the three test parts was made to close tolerances to ensure equal flow and part weight. The coupons were a one-quarter length segment of the engine seal pin geometry.

A Sorvall model RC2-B floor centrifuge was modified to provide the high-speed rotating drive and containment shroud for the rotating chamber. The centrifuge had a variable-speed drive with a maximum speed of 20,000 rpm; however, for the rotating test facility, the rotating test speeds were 500 rpm ($\Omega = 0.002$) and 10,300 rpm ($\Omega = 1$). A hole was cut out in the centrifuge lid to permit the air and particle supply pipe and instrumentation to be connected to the rotating chamber and to provide an exhaust to the laboratory atmosphere.

For the $\Omega = 0.002$ tests, two type-E thermocouples and two small stainless steel tubes for pressure measurement were inserted into the inside of the rotating chamber, as shown in Fig. 6. As in the static test facility, the measured total pressure upstream of the seal pin region was used in conjunction with the measured air mass flow rate and temperature to calculate the flow function for the test geometry. For the $\Omega = 1$ tests, excessive heating and rubbing due to rotational friction made it necessary to move the pressure taps and thermocouples located inside the chamber to a location further upstream. The pressure taps were moved to the tee fitting just above the rotary union, and the thermocouple at the inlet to the LFE was used as the upstream total temperature. Error from moving the pressure tap to an upstream location was determined to be negligible, since the pressure drop through the

upstream pipe nipple and rotary union was estimated to be about 24.9 Pa, or about 0.04% of the differential pressure across the test coupons. Additionally, the dynamic pressure at the upstream measurement location was about 0.01% of the total pressure.

The rotational pressure ratio across the test coupons and the rotational flow function were calculated using the parameter definitions in Eqs. (2) and (3). The seal pin and slot act to restrict the air flow passing through the platform gap much like that of flow through a nozzle. Air flow through a nozzle at the operating pressure and temperature conditions within this study can be accurately approximated as isentropic flow using the ideal gas equations. The analysis also assumes steady flow with constant specific heats and a sufficiently large upstream chamber to be considered a plenum. For the case of a rotating orifice or nozzle, Maeng et al. [12] have shown experimentally that there is additional energy imparted to the flow through transfer of angular momentum from the nozzle. Their study showed that an energy balance performed on a control volume including a rotating nozzle and its surroundings yields Eqs. (4)–(6) below.

$$PR_{rot} = \frac{P_{0,rot}}{p_b} \tag{2}$$

$$FF_{rot} = \frac{\dot{m}\sqrt{T_{0,rot}}}{P_{0,rot}} \tag{3}$$

$$P_{0,rot} = P_0\left(1 + \frac{T_{rot}}{T_0}\right)^{\frac{\gamma}{\gamma-1}} \tag{4}$$

$$T_{0,rot} = T_0 + T_{rot} \tag{5}$$

$$T_{rot} = \frac{(r \cdot \omega)^2}{2c_p} \tag{6}$$

The downstream pressure tap that was used to measure the differential pressure across the rotating test coupons was installed flush with the inside diameter of the ballistic wall, as shown in Fig. 6, about 8 cm radially outward from the outer diameter of the chamber and the exit of test coupons. It was, therefore, necessary to correct for the pressure difference between the measured pressure at the ballistic wall (p_w) and the back pressure at the exit of the test coupons (p_b).

To correct for this pressure difference, flow outside the rotating chamber was assumed to behave as a free vortex (irrotational fluid elements) for which the Bernoulli equation can be applied between any two points in the flow field. The Bernoulli equation written for locations just downstream of the rotating test coupons and near the ballistic wall can be reduced to the expression given in Eq. (7). The flow field velocity just downstream of the rotating chamber can be approximated by the velocity of the rotating chamber wall, while the flow field velocity near the ballistic wall is negligible (compared to the flow velocity near the rotating chamber wall when spinning). Incompressible flow with constant density was also assumed. Equation (7) can be solved for the back pressure p_b at the seal pin slot exit. Within Eq. (7) the density of the flow at the test geometry exit was approximated from the ideal gas relation in Eq. (8).

$$\frac{p_b}{\rho_b} + \frac{(r \cdot \omega)^2}{2} = \frac{p_w}{\rho_b} \tag{7}$$

$$\rho_b = \frac{p_w}{R \cdot T_w} \tag{8}$$

For the $\Omega = 0.002$ tests, this pressure correction value was approximately 0.03% of the pressure drop from the upstream rotating chamber to the ballistic wall for a $PR_{rot} = 1.6$. For the $\Omega = 1$ tests, the pressure correction value was approximately 19% of the pressure drop from the upstream rotating chamber to the ballistic wall for a $PR_{rot} = 1.6$. Similarly, for the $\Omega = 1$ tests at $PR_{rot} = 1.6$, the contribution of T_{rot} was approximately 6% for the value of PR_{rot} and 5% for the value of FF_{rot}.

Inside the rotating chamber, a horizontal circular plate with curved vertical walls was installed to direct the rust particles into the test coupons. This diffuser plate, shown schematically in Fig. 8(*a*) and in a photograph in Fig. 8(*b*), guided the rust particles toward the three test part regions in order to avoid a buildup of rust particles at the center of the diffuser plate. Both particle diffuser plates were symmetric and installed level at a consistent height.

Uncertainty and Repeatability. An uncertainty analysis of experimentally measured parameters was performed using the partial derivative method as described by Beckwith et al. [13]. Results shown in Tables 2 and 3 give nominal parameter values and their respective uncertainties for low and high pressure ratios tested. The uncertainty in flow function was mainly driven by bias uncertainties in the pressure and temperature measurements at the LFE. Both the flow function and reduction in flow function uncertainties increased as pressure ratio decreased due to the instrument bias uncertainties.

Each particle injection test for a given pressure ratio and injected rust mass was repeated a minimum of three times to insure repeatability of the blockage. After performing a 25-case repeatability study, Walsh et al. [14] concluded three repetitions of each test optimized testing efficiency and yielded repeatable reductions in flow function to within 7%. For the static tests, a 15-case repeatability study performed for $PR = 1.15$ and $m_{rust} = 0.089$ g showed three repetitions of each test yielded reductions in flow function to within 9%. In the rotating facility, each rust injection test measured the flow blockage through three identical test geometry parts. For statistical analysis, the flow blockage from each test in the rotating facility was considered to be an average of three tests. Analysis of nine rotating tests (three tests of three parts each) indicated the reduction in flow function was repeatable to within 7%. All repeatability results are reported for a 95% confidence interval.

Flow Blockage Results for Static Tests

Baseline flow parameters as a function of pressure ratio across the seal pin gap for the static blade testing are shown in Fig. 9 for several different conditions. The original experimental data were acquired after numerous assembles and disassembles. The second set of data, indicated as "retest experimental data" was an example dataset taken after the part was cleaned from the rust injection. The reduction in flow parameter was determined relative to the baseline data at a fixed pressure ratio.

The results with injection indicated that substantial quantities of rust were deposited in the blade platform area upstream of and at the seal pin slot. After performing injection tests, it was possible to reclaim deposited rust particles by carefully brushing them from the seal pin area and upstream blade platform surfaces. Comparing the mass of the reclaimed particles with the injected mass showed that about 80% of the injected rust mass was deposited near the seal pin area and the upstream blade platform surfaces. The percentage of reclaimed rust was relatively insensitive to the pressure ratio at which the rust was injected.

Figure 10 indicates the phenomena that occur after rust is injected through the seal pin gap. There is a notable decrease in the flow rate while the pressure ratio remained fairly constant. The decrease in flow rate remained constant in time so a reduction in the flow rate through the seal pin gap was discerned. The overall reduction in flow rate that occurred was then compared to the baseline presented in Fig. 9 to give an overall reduction in the flow function for the seal pin.

Results for the reduction in the flow blockage, shown in Fig. 11, indicated that the blockage increased with increased levels of rust injection and with increased pressure ratio for a given rust amount. It was expected that there be an increased flow blockage with increased rust injection. For the increased blockage at higher pressure ratios, inertial effects of the particles were

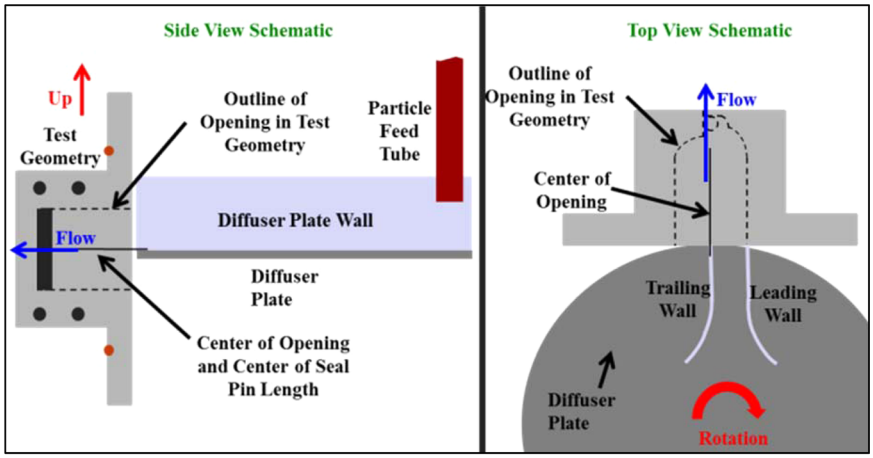

(A)

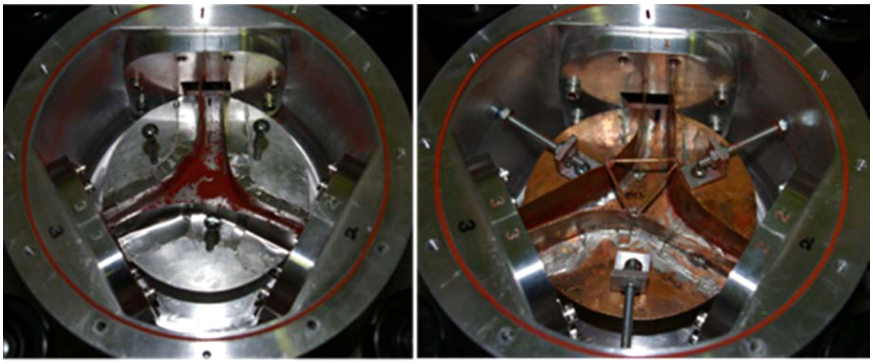

(B)

Fig. 8 Particle diffuser plate used during the rotating tests (*a*) schematic and (*b*) photographs

Table 2 Parameter uncertainties for static tests

	Value	% Uncertainty	Value	% Uncertainty
PR	1.05	0.09	1.59	0.69
$\dot{m}$ (kg/s)	7.15E-05	2.4	4.63E-04	1.5
FF (m-s-K$^{1/2}$)	1.21E-08	3.1	5.19E-08	2.1
RFF	13%	23	37%	3.9
m_{rust} (g)	0.039	2.6	0.232	0.43

considered. At high pressure ratios, increased fluid velocities inhibited the particles from following the flow streamlines, resulting in more impacts than at low pressure ratio slower velocity cases, leading to increased deposition and greater flow blockage.

Moving through the blade platform area in the direction of coolant flow, the flow area narrowed from a maximum near the root to the minimum area at the seal pin; therefore, even for particle injection at a constant pressure ratio, particle behavior was anticipated to become progressively more ballistic as particles moved towards the seal pin flow area with increased fluid velocity. The existence of ballistic particle behavior was confirmed through visual observation of particle depositions and analysis of deposition samples via environmental scanning electronic microscope (ESEM).

Figure 12 shows the locations where rust particle deposition was inspected, and Fig. 13 shows ESEM images of rust taken from each location after disassembly. By visual inspection, it was observed that the largest particles were only present at the larger flow area between the seal pin and the blade root. The smallest particles, appearing as a finely ground powder, were only present at the narrowest flow area where the seal pin contacted the front blade platform. Particle size analyses were performed on ESEM particle images to further investigate the visually observed variation in particle size with deposition location.

Deposition samples taken from various locations on the front blade, rear blade, and seal pin confirmed the ballistic behavior, as

Table 3 Parameter uncertainties for rotating tests

	Value	% Uncertainty	Value	% Uncertainty
ω (rpm)	514 ± 3	0.5	10342 ± 2	0.02
PR_{rot}	1.14 ± 0.02	1.6	1.61 ± 0.02	1.3
FF_{rot} (m-s-K$^{1/2}$)	3.64E-08 ± 1.15E-09	3.2	3.20E-08 ± 9.15E-10	2.9
RFF	21% ± 6.6%	32	22% ± 2.5%	11
m_{rust} (g)	8.034 ± 0.003	0.04	8.017 ± 0.002	0.02

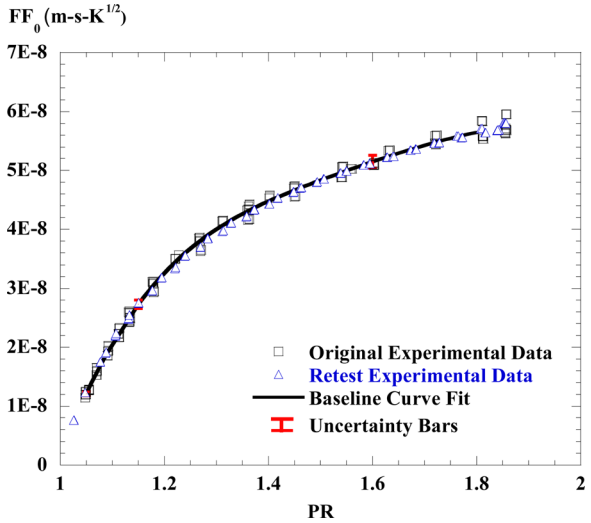

Fig. 9 Baseline flow function for seal pin gap before (original) and after (retest) rust injection tests

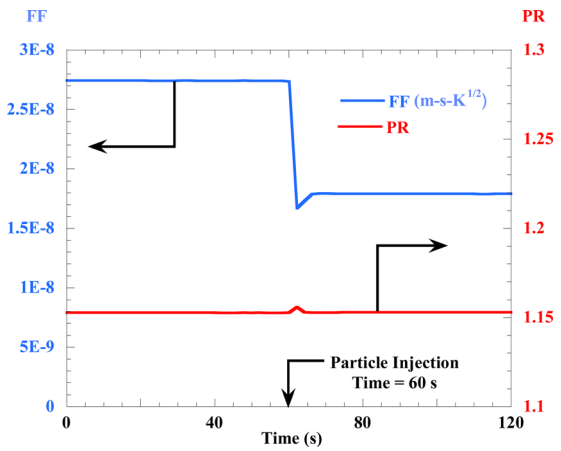

Fig. 10 Flow function as a function of time before and after particle injection

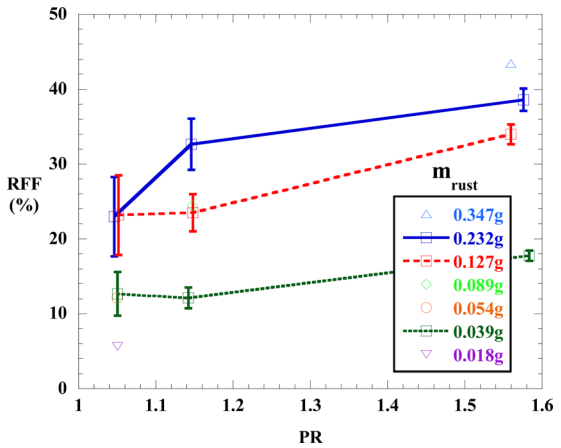

Fig. 11 Reduction in flow due to rust injection for the static testing

shown in Fig. 13. The largest particles ($>100\,\mu$m) were present only in the preinjection location and in sample location 5 from the rear blade contour. Downstream samples from the seal pin slot, seal pin, and seal pin contact area (sample locations 3, 5, and 1, respectively) had particles no larger than $100\,\mu$m. Absence of large particles in the downstream samples from the narrowest flow areas suggests that large particles impacted with upstream surfaces and either were deposited or rebounded. Particle erosion and breakage occurred for the rebounding particles so that, progressing from the root towards the seal pin, sizes of suspended particles became increasingly smaller.

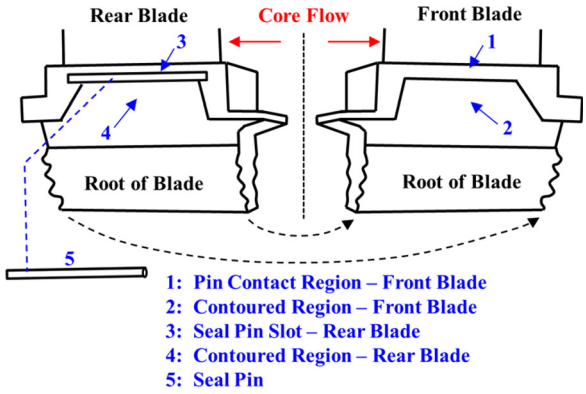

Fig. 12 Blade locations for ESEM particle analysis

Flow Blockage Results for Rotating Tests

Results from rust injection tests performed in the rotating test facility are presented in this section. As was discussed, the test parts (coupons) represented a one-quarter length section of the full-scale engine hardware tested in the static test facility. The effects of pressure ratio and rotation were investigated, with some tests performed at a low rotating speed ($\Omega = 0.002$) and others performed at conditions matching the engine centrifugal acceleration ($\Omega = 1$).

Tests in the rotating facility were performed with three identical test parts open to flow and particle deposition; therefore, the flow blockage measured in each test was considered an average of the blockage in the three parts. For the test geometry, the clean flow function was measured over a range of pressure ratios at a centrifugal acceleration relative to the engine $\Omega = 0.002$, first for each part individually and then for all three parts open to flow simultaneously. Multiple assemblies of the test geometries and seal pins were performed to show the baseline flow function was repeatable. As shown in Fig. 14, the baseline flow function for each part was similar and matched the one-third-scale flow function for flow through all three parts. These results indicate all parts were identical. Note the single part baseline curve is an average curve for all the data.

Shown in Fig. 15, baseline flow function curves were generated for $\Omega = 0.002$ (500 rpm) and $\Omega = 1$ (10,300 rpm) with all three identical coupons open to flow (flow is three times that of a single part). As in the static tests, the baseline curve was used to compute the reduction in flow function after injecting rust particles. At $\Omega = 1$, the flow area was reduced due to the increased outward radial force pressing the seal pins into the slots. The resulting smaller flow area was responsible for the decrease in flow function at $\Omega = 1$ relative to the $\Omega = 0.002$ baseline.

Significant quantities of rust particles deposited in the test geometries. In contrast with the static test facility, a measurable amount of rust also deposited in the particle feed pipe and on surfaces upstream of the test geometry parts. After each rust injection test, rust particles were removed from the rotating test facility by tapping, brushing, and blowing with compressed air. The mass and location of collected particles was recorded. Generally more than 95% of the total injected rust mass was collected from the particle feed pipe, diffuser plate, chamber walls and part flanges, and from inside the test geometry parts. Deposition inside the test coupons included all rust deposited on the contoured surfaces

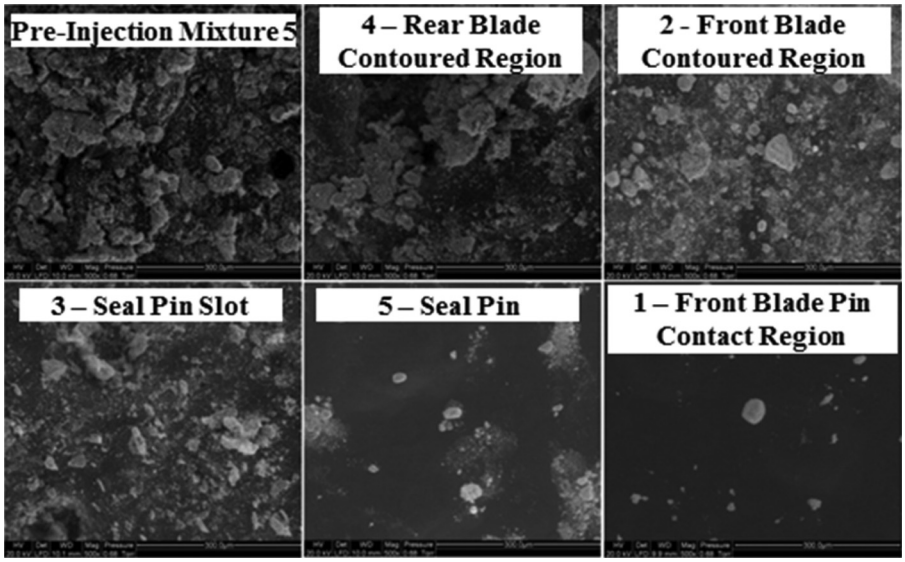

Fig. 13 ESEM images of rust at 500× magnification; sample numbers correspond with Fig. 12. Across top row (left to right) is shown preinjection; locations 4 and 2. Across the bottom row is locations 3, 5, and 1.

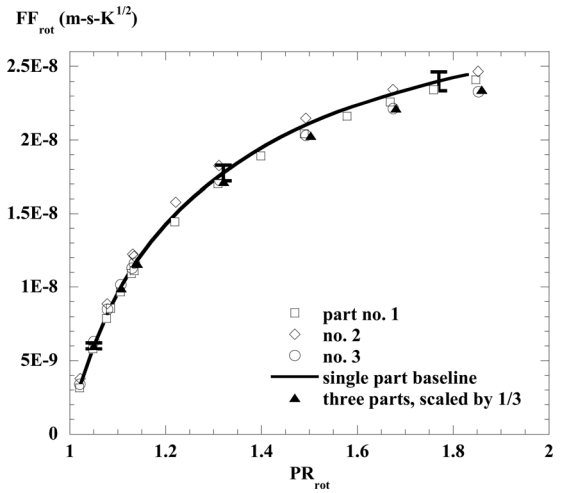

Fig. 14 Baseline flow function as a function of pressure ratio for the rotating tests with a single test part open to the flow at $\Omega = 0.002$

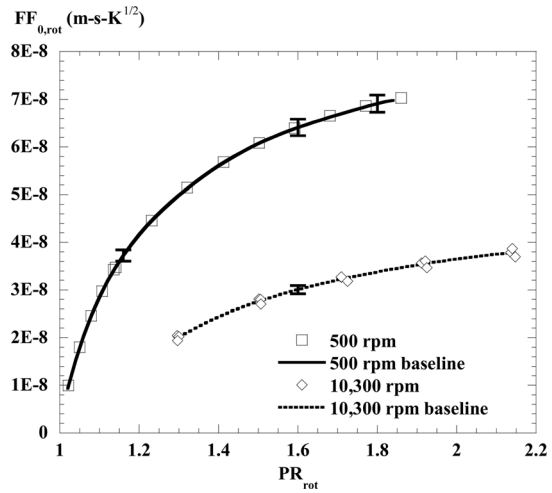

Fig. 15 Baseline flow function as a function of pressure ratio for the rotating tests, with all the three test parts open to the flow at both $\Omega = 0.002$ and 1.0 (curves are best fits to data)

leading into the seal pin slot and rust surrounding the seal pin. Very little rust passed through the test geometry parts to the atmospheric downstream chamber.

Shown in Table 4 is a test matrix that was developed for the rotating study to investigate the effects of rotating speed and pressure ratio on rust deposition and flow blockage. Tests were performed at pressure ratios of 1.15, 1.6, and 1.8. Injecting rust amounts with a mass loading ratio MLR (mass of rust relative to mass flow rate of air) similar to the static tests of about 0.5 s resulted in negligible flow blockage, so the rust amounts were increased to yield flow blockages similar to what was observed in the static tests.

Although the pattern of the main rust buildup was similar at $\Omega = 0.002$ and $\Omega = 1$, certain aspects of the deposition were affected by the increased centrifugal acceleration at $\Omega = 1$. As shown in Fig. 16, the surfaces leading to the seal pin were relatively clean at $\Omega = 0.002$ but were coated with a thin layer of very fine rust particles at $\Omega = 1$.

Inside the spinning chamber, the motion of the air is similar to that of a solid body. Particles entering this air were subjected to centrifugal and Coriolis acceleration forces. The rotation accelerated larger, more massive particles radially outward so rapidly that the Coriolis acceleration had little effect in increasing their circumferential velocity. Smaller particles; on the other hand, were less-rapidly accelerated in the outward radial direction such that there was more time for the Coriolis acceleration to increase their circumferential velocity towards that of the fluid. In addition, smaller particles tended to follow the flow more readily since the time scale for their momentum change was much shorter. For these reasons, only the smaller particles deposited on the leading surfaces while the larger particles formed the bulk of the deposition on the trailing surfaces.

Due to the increased centrifugal acceleration at $\Omega = 1$, the particles compacted to form hardened conglomerations as large as 12 mm, which is contrasted in Fig. 16 with the relatively loose particles removed after a test at $\Omega = 0.002$. Deposits formed for $\Omega = 0.002$ could be easily removed from the parts by gentle tapping and brushing. At $\Omega = 1$, vigorous tapping and brushing was

Table 4 Mass loading ratios for rotating tests

	Ω = 0.002			Ω = 1		
PR_{rot}	Mass flow rate (kg/s)	Rust mass (g)	MLR (s)	Mass flow rate (kg/s)	Rust mass (g)	MLR (s)
1.15	2.32E-04	0.4 6.5	1.7 28			
1.6	5.76E-04	0.4 6.6	0.7 11	2.62E-04	1.6 6.7	6.1 26
1.8	6.99E-04	0.4 6.7	0.6 10			

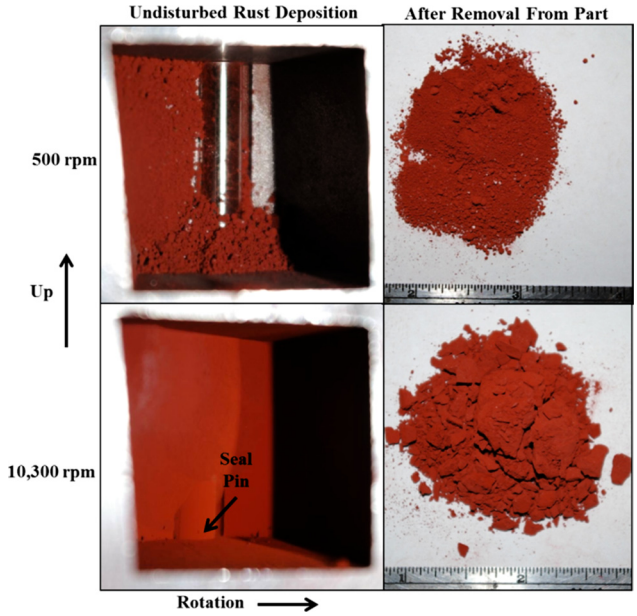

Fig. 16 Rust deposition for 1500 and 10,300 rpm (view of test geometry in outward radial direction)

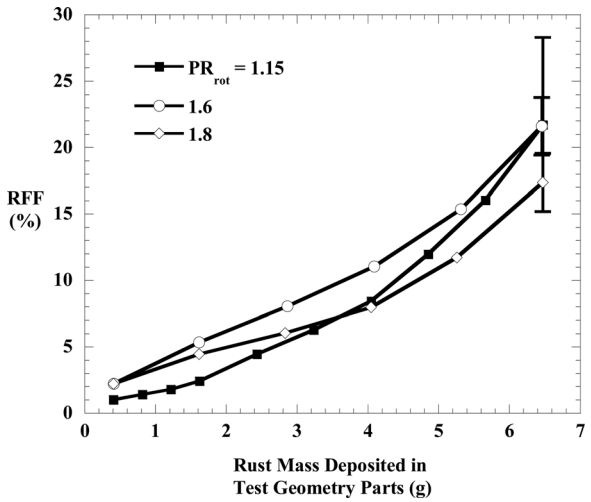

Fig. 17 Flow blockage results for the rotating tests when Ω = 0.002 at various pressure ratios

required to remove particles from the parts, and large conglomerations of particles remained even after being removed.

To investigate the effect of pressure ratio on flow blockage under rotating conditions, rust was injected at pressure ratios of 1.15, 1.6, and 1.8 at Ω = 0.002. Results for these tests are shown in Fig. 17, where the deposited rust mass is based on the proportion of total injected rust found in the test geometry parts at the end of the test and thus excludes rust deposited elsewhere in the test facility. Flow blockage was nearly independent of pressure ratio. This finding is in contrast with the results from the static testing, for which blockage increased with pressure ratio due to increasingly ballistic particle behavior. Ballistic particle behavior was also observed in the rotating tests; however, the centrifugal forces governed this behavior, dominating any effect from the increased fluid velocity at higher pressure ratios.

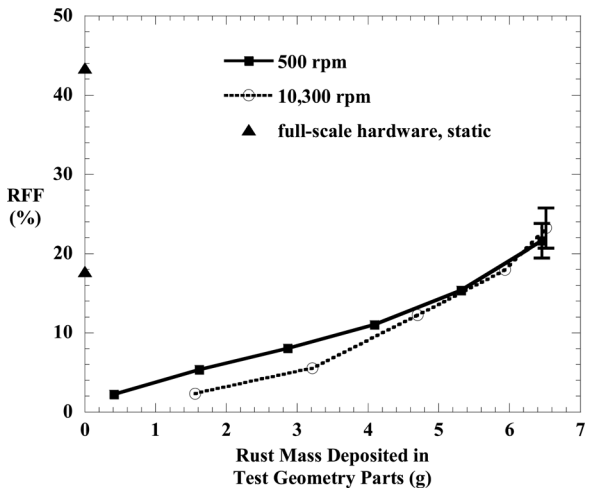

Fig. 18 Flow blockage results for the rotating tests at both Ω = 0.002 and Ω = 1 for PR_{rot} = 1.6

Because the pressure ratio did not have a significant effect, the rotational effects were only measured at a PR = 1.6. As shown in Fig. 18, flow blockage behavior was also similar at the two different rotational speeds with centrifugal accelerations Ω = 0.002 and Ω = 1. The range of flow blockage for the static tests is shown on the mantissa of Fig. 18 for reference. Note that the rust mass amounts were significantly lower than for rotating tests, which is why the range of results are shown near zero grams of rust.

The results in Fig. 18 indicate significant overall effects of any rotation, whether it be low or high values. First, as was indicated, the rust amounts needed for the rotating coupons was more than an order of magnitude higher than for the static airfoil tests. Second, it was shown that even with the lower rust injection amounts, the blockage measured was greater for the static case than for the rotational case. Third, the results indicated a preferential location for the particular rust to be deposited. Most of the rust that blocked the seal pin area was found to be on the trailing portion of the seal pin rather than the leading portion.

Conclusions

Rust deposition for an axial seal pin was investigated on static blades from a gas turbine engine and on rotating coupons of a sector of the blades. Rust composed primarily of red iron oxide was characterized in separate experiments at temperatures and centrifugal accelerations representative of an industrial gas turbine operating at base load conditions. Results indicated particles were unaffected in their appearance and size distribution when heated up to 850 °C. After spinning at engine representative centrifugal acceleration, rust particles exhibited significant compaction to twice that of the loose bulk density. These findings indicated that, for particles entrained in air flow near the axial seal pin, centrifugal acceleration was an important parameter.

Rust injection experiments performed in the static test facility yielded significant flow blockages up to 40%. These static results indicated that particle deposition in the seal pin gap has a significant role in reducing leakage flow. The pressure ratio strongly influenced deposition. Particle breakage and erosion were observed indicating particles tended to impact surfaces due to the inability to follow flow streamlines. Visual observation and particle size analysis revealed only the smallest particles were deposited in the narrowest flow areas at the seal pin, which underscores the challenge of preventing particle deposition in the seal pin slot since the smallest particles are the most difficult to filter from the cooling air.

For rotating tests performed even at very low centrifugal acceleration relative to engine conditions, the centrifugal and Coriolis accelerations were shown to dominate the effect of pressure ratio. The measurements indicated that significantly larger amounts of rust were needed under rotating conditions than static conditions for similar blockage reductions to occur. Rotation caused particles to initially build up on the trailing surface of the seal pin slot. Observations of the data indicated that when rotational effects were matched to that of the engine, particles were compacted into large conglomerations with the potential to inhibit motion of the seal pin.

Nomenclature

a_c = centrifugal acceleration
A = area
b = back or downstream
c_p = specific heat
e = engine
FF = flow function: $FF = \dot{m}\sqrt{T_0}/P_o \quad (m \cdot s \cdot K^{1/2})$
FF_0 = baseline flow function
g = gravitational acceleration
LFE = laminar flow element
L_{sp} = seal pin length
$\dot{m}$ = mass flow rate
m_{rust} = rust mass
M = Mach number
P_0 = total pressure
p = static pressure
PR = pressure ratio: $PR = P_0/p_b$
r = radius
R = gas constant
RCF = relative centrifugal forces: $r \cdot \omega^2/g$
RFF = reduction in flow function: $RFF = 1 - FF/FF_o$
T_0 = total temperature
T = static temperature
γ = ratio of specific heats
ω = rotational speed
Ω = acceleration relative to engine: $\Omega = a_c/a_{c,e}$
ρ = density

References

[1] Wright, I. G., and Gibbons, T. B., 2007, "Recent Developments in Gas Turbine Materials and Their Implications for Syngas Firing," Int. J. Hydrogen Eng., **32**, pp. 3610–3621.
[2] Patel, S., 2009, "Mitsubishi Wraps Up Development of J-Class Mega Turbine," Power, July 1, http://www.powermag.com/issues/departments/global_monitor/Mitsubishi-Wraps-Up-Development-of-J-Class-Mega-Turbine_2010.html
[3] Schneider, O., Dohmen, H. J., and Reichert, A. W., 2002, "Experimental Analysis of Dust Separation in the Internal Cooling Air System of Gas Turbines," ASME Paper No. GT2002-30240.
[4] Schneider, O., Dohmen, H. J., Benra, F.-K., and Brillert, D., 2003, "Investigations of Dust Separation in the Internal Cooling Air System of Gas Turbines," ASME Paper No. GT2003-38293.
[5] Schneider, O., Dohmen, H. J., Benra, F.-K., and Brillert, D., 2004, "Dust Separation in a Gas Turbine Pre-Swirl Cooling Air System: A Parameter Variation," ASME Paper No. GT2004-53048.
[6] Dunn, M., Padova, G. C., Moller, J. E., and Adams, R. M., 1987, "Performance Deterioration of a Turbofan and a Turbojet Engine Upon Exposure to a Dust Environment," ASME J. Eng. Gas Turb. Power, **109**, pp. 336–343.
[7] Batcho, P. F., Moller, J. D., Padova, C., and Dunn, M. G., 1987, "Interpretation of Gas Turbine Response Due to Dust Ingestion," ASME J. Eng. Gas Turb. Power, **109**, pp. 344–352.
[8] Dunn, M., Padova, G. C., and Adams, R. M., 1987, "Operation of Gas Turbine Engines in Dust-Laden Environments," Advisory Group for Aerospace Research and Development (AGARD)-Advanced Technology of Aero Engine Components, Paris, May 4-8.
[9] Kim, J., Dunn, M. J., Baran, A. J., Wade, D. P., and Tremba, E. L., 1993, "Deposition of Volcanic Materials in the Hot Sections of Gas Turbine Engines," ASME J. Eng. Gas Turb. Power, **115**, pp. 641–651.
[10] Weaver, M. M., Dunn, M. G., and Heffernan, T., 1996, "Experimental Determination of the Influence of Foreign Particle Ingestion on the Behavior of Hot-Section Components Including Lamilloy," ASME Turbo Expo, Birmingham, UK, June 10–13, ASME Paper No. 96-GT-337.
[11] Dovali, F., 2006, "Rotor Air System Particulate Testing at AEC Vann Unit 2," Siemens Power Generation, Siemens EC-06171.
[12] Maeng, D. J., Lee, J. S., Jakoby, R., Kim, S., and Wittig, S., 1999, "Characteristics of Discharge Coefficient in a Rotating Disk System," ASME J. Eng. Gas Turb. Power, **121**, pp. 663–669.
[13] Beckwith, T. G., Marangoni, R., and Lienhard, J. H. V., 1993, *Mechanical Measurements*, Addison Wesley, New York.
[14] Walsh, W. S., Thole, K. A., and Joe, C., 2006, "Effects of Sand Ingestion on the Blockage of Film-Cooling Holes," ASME Paper No. GT2006-90067.